Calculation and Experimental Validation of Induced Currents on Coupled Wires in an Arbitrary Shaped Cavity

KORADA R. UMASHANKAR, SENIOR MEMBER, IEEE, ALLEN TAFLOVE, SENIOR MEMBER, IEEE, AND BENJAMIN BEKER, STUDENT MEMBER, IEEE

Abstract—**An efficient numerical technique is presented for the calculation of induced electric currents on coupled wires and multiconductor bundles placed in an arbitrary shaped cavity and excited by an external incident plane wave. The method is based upon the finite-difference time-domain (FD-TD) formulation. The concept of equivalent radius is used to replace wire bundles with single wires in the FD-TD model. Then, the radius of the equivalent wire is accounted by a modified FD-TD time-stepping expression (based on a Faraday's law contour-path formulation) for the looping magnetic fields adjacent to the wire. FD-TD computed fields at a virtual surface fully enclosing the equivalent wire are then obtained, permitting calculation of the currents on the wires of the original bundle using a standard electric field integral equation (EFIE). Substantial analytical and experimental validations are reported for both time-harmonic and broad-band excitations of wires in free space and in a high-Q metal cavity.**

I. Introduction

RECENT INTEREST IN potential defense applications of high-power microwaves (HPM) has added another dimension to the long-time problem of electromagnetic wave coupling to wires within conducting cavities. Essentially, the power-bandwidth product of HPM illumination can be sufficiently high that substantial wide-band coupling can occur despite normal shielding practices. Complex aperture coupling phenomena, such as path length resonances, may greatly enhance power transmission through narrow slots and lapped joints in thick conducting screens, as reported in a companion paper [1]. Aperture resonances may couple in a very complex way to internal, volume-type cavity resonances, which in turn might excite resonant modes along wires and wire bundles embedded within the cavity. A necessary goal of any analytical or numerical modeling approach for this problem is to achieve a self-consistent composition of the coupling physics of the apertures, cavities, and internal wires or bundles that are commonly found in engineering designs.

Detailed treatments of coupling to a wire behind a slot aperture in an infinite, planar, conducting screen have appeared in the literature [2]–[4]. These treatments are based upon frequency-domain, integral equation approaches, with solution via the method of moments, and have investigated coupling resonances due to slot width, wire length, wire-slot separation, and wire-slot orientation angle. The effects of screen curvature into a cylindrical cavity with a longitudinal slot aperture have been reported for the two-dimensional case [5]. Here, interior and exterior eigenmode expansions for the fields are matched at the aperture, with the addition theorem used to account for the possibility of the internal wire not being centered in the cavity.

General three-dimensional numerical models of coupling to wires in arbitrary cavities have been based upon the finite-difference time-domain (FD-TD) approach [6], [7]. In [6], the emphasis was on the use of an equivalence theorem presented by Schelkunoff [8] to achieve a useful decoupling of the exterior and interior problems for wave penetration through an aperture into a cavity. Wire modeling there was relatively primitive, treating a thin wire or wire bundle (having cross-section diameter less than one space cell) as a single equivalent conducting cylinder of square cross section spanning exactly one cell. No attempt was made to obtain more than an estimate of common-mode current on a bundle; evaluation of individual wire currents taking into account terminations and interconnections was not possible. Further, although the feasibility of constructing a highly realistic FD-TD model of a complex engineering structure (missile seeker section) was demonstrated, there were no experimental studies of the accuracy of the predicted common-mode cable currents for this model.

In [7], a more sophisticated FD-TD treatment of thin wires was presented. This treatment was based upon the assumption of a $1/r$ dependence of the magnitude of local fields with radial distance r from the wire center (for $r < 0.1$ wavelength), and introduction into integral forms of Maxwell's equations to obtain modified FD-TD formulas to simulate the presence of a wire. However, this work emphasized the development and use of an "in-cell inductance" model of the thin wire, essentially a lumped-parameter wire model where the current distribution was obtained via solution of a differential equation for the wire current solved concurrently with the FD-TD time stepping. Multiple, closely coupled wires (such as those in a wire bundle) could be modeled in this manner by solving simultaneous, coupled equations for the time-dependent wire

Manuscript received June 5, 1986; revised February 25, 1987. This work was supported in part by Lawrence Livermore National Laboratory under Contract 6599805, and by National Science Foundation Grant ECS-8515777.

K. R. Umashankar and B. Beker are with the Department of Electrical Engineering and Computer Science, University of Illinois, Chicago, IL 60680.

A. Taflove is with the Department of Electrical Engineering and Computer Science, Technological Institute, Northwestern University, Evanston, IL 60201.

IEEE Log Number 8716771.

currents concurrently with the FD-TD time stepping. This approach was difficult to implement because of numerical instabilities involved in the simultaneous execution of the coupled electromagnetic field and wire current partial differential equations.

The goal of this paper is to describe a recently developed advance in FD-TD modeling of wires and wire bundles, relative to the work of [6] and [7], which approaches a self-consistent treatment of wire and cavity physics for realistic engineering problems of contemporary interest. This advance is based on four key elements.

1) *Equivalent radius*: For purposes of accounting the physics of a bundle of closely spaced, parallel wires at points exterior to the bundle, the bundle is replaced by a single wire having a properly defined equivalent radius [9], [10]. In particular, if the bundle cross-section diameter is electrically small, a simple expression for the equivalent radius is obtained which is independent of frequency.

2) *Wire subcell model*: A Faraday's law contour integral approach is used to obtain a simple modification of the basic FD-TD algorithm to properly model the electromagnetic field near the wire of 1), even when the equivalent radius is much less than one FD-TD space lattice cell [1].

3) *Virtual surface*: A virtual surface is introduced which completely encloses the equivalent-radius wire of 1). The physics of the presence of the wire within the virtual surface is accounted by implementing the wire subcell model of 2) at FD-TD azimuthal magnetic field points immediately adjacent to the equivalent wire. Now, the total tangential E- and H-fields at points along the virtual surface (computed using FD-TD) are identical to the actual field values at the corresponding space locations in the presence of the original wire bundle. These tangential fields on the virtual surface are converted into corresponding equivalent electric and magnetic current sources. According to electromagnetic equivalences, these current sources are the only data required to calculate the total fields inside of the virtual surface.

4) *Electric field integral equation (EFIE)*: An EFIE is applied to compute the unknown induced electric current distribution along the wires of the original bundle using the virtual-surface equivalent current sources of 3) as excitation. The integral equation is solved based on the method of moments numerical technique [11]. Note that the solution space of the EFIE is limited to the unknown currents along the wires of the bundle, thereby limiting the size of the required method-of-moments solution matrix.

The above procedure is aimed at applying the FD-TD and EFIE analyses to appropriate parts of the overall coupling problem. Namely, the volumetric modeling capabilities of FD-TD are exploited to efficiently account for the physics of cavities having arbitrary shape and loading. And, the detailed wire modeling capabilities of EFIE are exploited to efficiently account for the physics of wire bundles having loads and interconnections. The accuracy and the corresponding self-consistency of this procedure hinges upon the use of a single wire of equivalent radius to represent the original wire bundle in the FD-TD analysis. This paper will provide examples of both free-space and cavity coupling problems which indicate that the accuracy of the modeling procedure is good to excellent, and useful for engineering applications.

In the following sections, a succinct discussion is presented regarding the equivalent radius of a wire bundle, the contour integral model of a single wire in an FD-TD space cell, the virtual surface enclosing the equivalent-radius wire, and the electric field integral equation. This paper will then report numerical and experimental validation studies for the new tool. The numerical studies involve modeling of the plane-wave excitation of coupled wires in free space, including bundles comprised of equal and unequal-length wires (some of resonant length), validated against the usual frequency-domain integral equation/method of moments approach. The experimental studies involve modeling of the plane-wave excitation of either a single wire or a pair of coupled wires centered within a finite, cylindrical, metal cavity having a resonant, circumferential, slot aperture, validated against measured data obtained at Lawrence Livermore Laboratory.

II. Equivalent Radius of Wire Bundle

The subject of electromagnetic equivalences as applied to wire cage antenna models has been previously studied [9], [10]. In [9], an equivalence was developed for a cage antenna consisting of identical conductors of finite length placed around a circle. The equivalence provided a single conductor of the same length, so that the total axial current distribution is the same in both cases. In [10], a comparatively more accurate analysis was developed for a loaded, infinitely long, cylindrical antenna, providing an equivalence for an infinitely long, loaded, wire cage antenna that yields the same radiated field. The analysis of [9] and [10] can be applied to a bundle of closely spaced, parallel wires, permitting replacement of the bundle by an *equivalent single wire* for purposes of accounting the physics of the bundle at points exterior to the bundle. In particular, if the bundle cross-section diameter is electrically small, a simple expression for the equivalent radius is obtained which is independent of frequency.

Fig. 1 illustrates the nature of the total-field equivalence problem. For simplicity, it is assumed that there exists a set of parallel, loaded, infinite-length wires within a single FD-TD space cell. Here, an equivalent single wire is defined such that the total external electrical field E^T and magnetic field H^T produced by the original bundle and the equivalent single wire are identical.

Consider first the electromagnetic behavior of the infinitely long, equivalent single wire of Fig. 1(c), assuming a wire orientation along the z-axis in an isotropic homogeneous medium, and illumination by a transverse magnetic (TM) polarized plane wave. The following notation is used:

ϕ_i	incident angle of plane wave excitation
ω	frequency of excitation
γ	jk, free-space propagation constant
b	radius of wire
η	free-space intrinsic impedance
R_w	resistance loading on wire per unit length
E_z^w	scattered electric field due to wire
H_ϕ^w	scattered magnetic field due to wire.

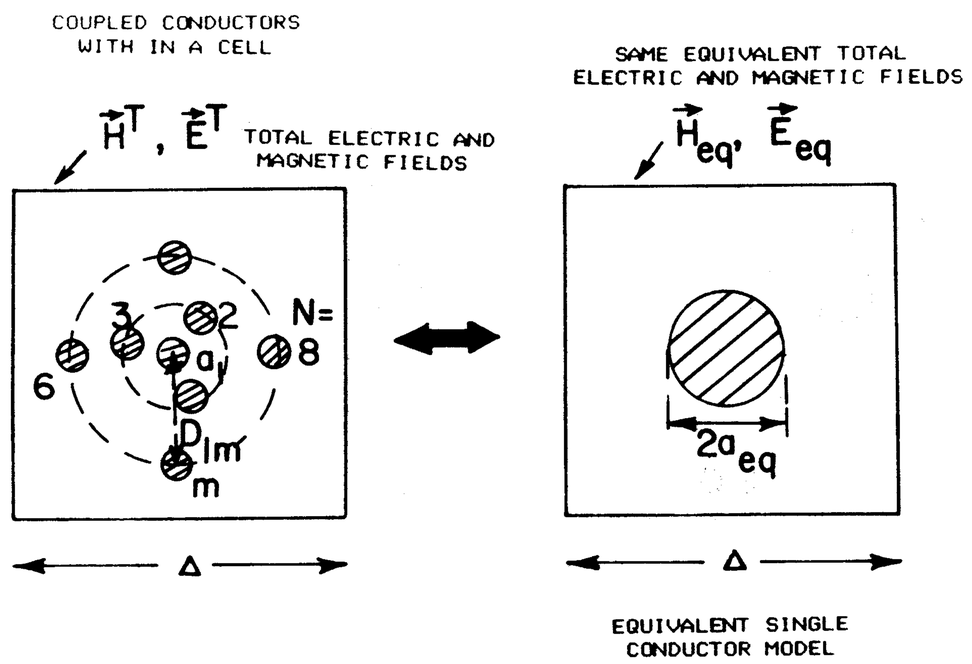

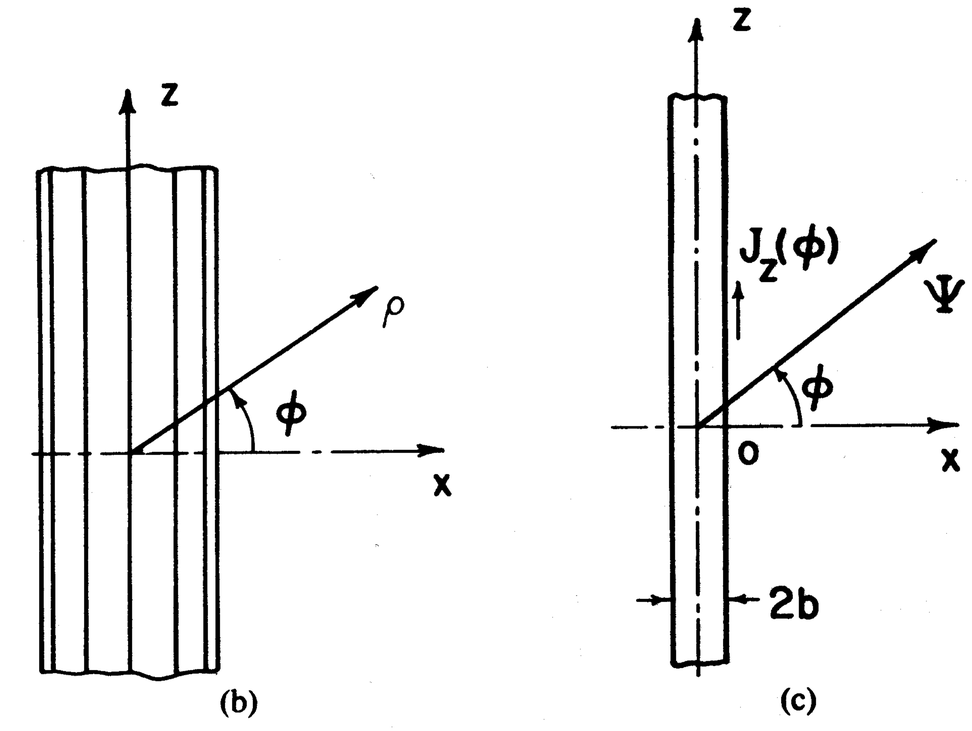

Fig. 1. Equivalence of wire bundle and single wire. (a) Cross-section geometry. (b) Original wire bundle, longitudinal view. (c) Equivalent single wire.

Assuming an exp $(j\omega t)$ time dependence for the field quantities, the plane wave excitation is given by

$$E_z^i(\rho, \phi) = E_0^i e^{-\gamma\rho \cos(\phi - \phi_i)}. \tag{1}$$

Treating the scattering by the wire as an impedance boundary value problem [10], the scattered electric and magnetic fields are given by

$$E_z^w(\rho, \phi) = E_0^i A_0(\omega) K_0(\gamma\rho) \tag{2a}$$

$$\eta H_\phi^w(\rho, \phi) = -E_0^i A_0(\omega) K_1(\gamma\rho) \tag{2b}$$

$$A_0(\omega) = \frac{-[I_0(\gamma b) - 2\pi b R_w I_1(\gamma b)/\eta]}{[K_0(\gamma b) + 2\pi b R_w K_1(\gamma b)/\eta]} \tag{2c}$$

where I_0, I_1 and K_0, K_1 are the zero-order and first-order modified Bessel functions.

Consider next the case of the original bundle (N parallel, infinitely long, loaded wires as shown in Fig. 1(b)). The following notation is used:

E_z^s	scattered electric field due to wire bundle
H_ϕ^s	scattered magnetic field due to wire bundle
a_n	radius of a wire in the bundle, with $\lvert\gamma a_n\rvert \ll 1$
(ρ_n, ϕ_n)	coordinate location of the nth wire
R_n^c	resistance loading on the nth wire per unit length.

Upon enforcing the impedance boundary condition on each wire of the bundle, the corresponding scattered electric and magnetic fields are obtained as

$$E_z^s(\rho, \phi) = E_0^i \sum_1^N T_n(\omega) K_0(\gamma \lvert\vec{\rho} - \vec{\rho}_n\rvert) \tag{3a}$$

$$\eta H_\phi^s(\rho, \phi) = -E_0^i \sum_1^N T_n(\omega) K_1(\gamma \lvert\vec{\rho} - \vec{\rho}_n\rvert) \frac{\partial}{\partial\rho}(\lvert\vec{\rho} - \vec{\rho}_n\rvert) \tag{3b}$$

where the coefficients T_n, for $n = 1, 2, 3, \cdots, N$ are obtained as a solution to the matrix equation given by

$$[T_n] = [S_{mn}]^{-1}[V_m]. \tag{4a}$$

In (4a), the matrix elements are given by

$$V_m = -[1 + 2\pi a_m R_m^c \cos(\phi_m - \phi_i)/\eta] e^{-\gamma\rho_m \cos(\phi_m - \phi_i)} \tag{4b}$$

$$S_{mn} = K_0(\gamma \lvert\vec{\rho}_m - \vec{\rho}_n\rvert), \qquad \text{for } m \neq n \tag{4c}$$

$$= K_0(\gamma a_m) + 2\pi a_m R_m^c K_1(\gamma a_m)/\eta, \qquad \text{for } m = n. \tag{4d}$$

The field coefficients T_n obtained from (4a), and the corresponding scattered electric and magnetic fields given by (3a) and (3b), are functions of angle ϕ. In fact, for electrically small bundle diameters, considerable simplification is possible. For a special case of identical wires located equidistant along the circumference of a circle to form a circular, cylindrical, loaded wire cage [9], [10], the T_n coefficients are all equal due to the circulant nature of the coupling matrix.

The key to accurate exploitation of the equivalent radius concept is the proper location of the virtual surface relative to the original wire bundle. This is illustrated in Fig. 2, which shows the near scattered field distribution (versus angle and radial distance) of a circular wire cage comprised of six parallel loaded wires. The cage has a radius $kA = 1$, with individual wires of radius $ka = 0.01$ and uniform loading of 50 Ω/m.[1] As Fig. 2(b) shows, the azimuthal magnetic field has intense peaking near the individual wires of the bundle. Clearly, a single equivalent wire cannot model this fine field structure. However, at 1.75 radii from the cage center, the spiked nature of the magnetic field is gone and a single equivalent wire can provide a good model. The virtual surface should be located no closer to the bundle than this to properly use the equivalent radius concept.

Given this constraint, we equate either (2a) and (3a) or (2b) and (3b) to obtain the equivalent radius of the wire bundle. This enforces the equivalence of the total electric and magnetic fields along a virtual surface enclosing the original wire bundle and its single-wire equivalent (in a region of uniform scattered fields). If the cross-section diameter of the bundle is electrically small (as for the case of a cross section contained within a

[1] The electrical distances assumed here can be scaled down, yielding similar results for bundles of electrically small cross sections.

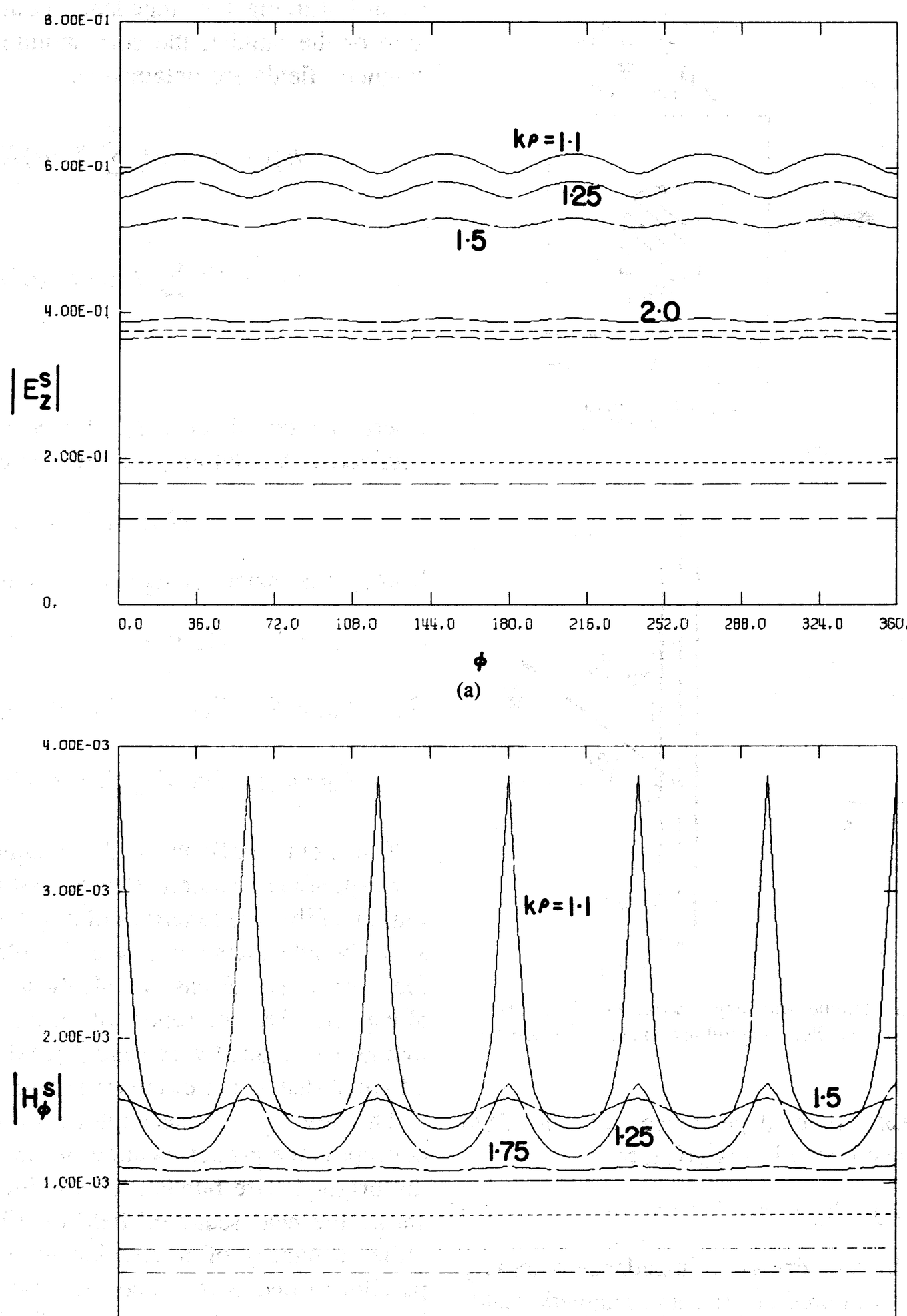

Fig. 2. Near scattered field distributions of circular wire cage versus angle and radial distance. (a) $|E_z^s|$. (b) $|H_\phi^s|$.

single FD-TD space cell), this yields a frequency-independent equivalent radius for the unloaded, uniform, wire-cage bundle:

$$a_{eq} = (a_1 D_{12} D_{13} D_{14} \cdots D_{1m} \cdots D_{1N})^{1/N} \tag{5}$$

where D_{1m} is the distance between conductors 1 and m [9], [10].

III. Contour Integral Model of a Single Wire in a Space Cell

The contour integral interpretation of the FD-TD analysis [1] permits incorporation of the near-field physics of a wire, yielding special-purpose FD-TD time-stepping expressions. Fig. 3 illustrates the Faraday's law contour path used to derive the special FD-TD algorithm for the circumferential magnetic field immediately adjacent to a single wire (taking $r_0 = a_{eq}$ to be the radius defined using the equivalent bundle model of Section II). Although Fig. 3 shows the wire cross section to be fully contained in one space cell, this approach is general and permits special magnetic field points to be computed even if the wire cross section overlaps adjacent cells [12]. Further, although only H_y is shown, the analysis can be easily generalized for the other circumferential magnetic field components.

The following briefly summarizes the assumptions concerning the near-field physics that are incorporated into the

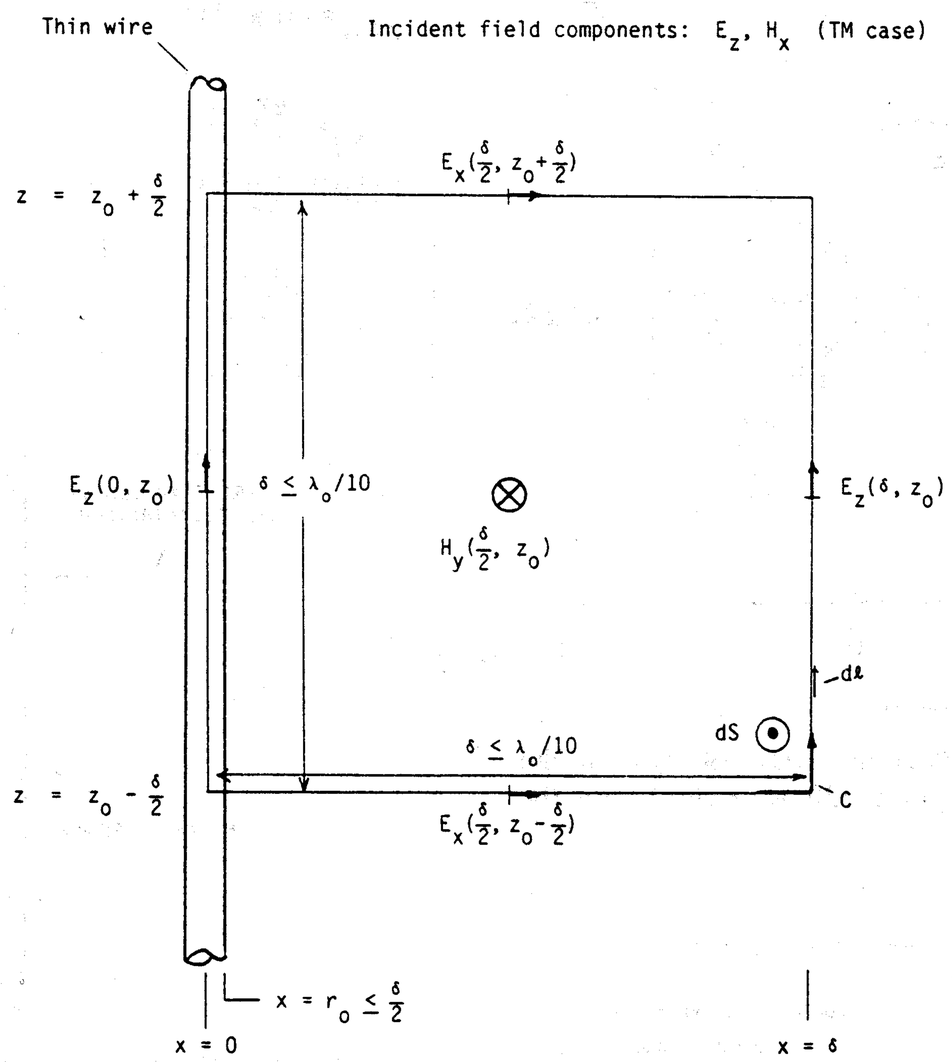

Fig. 3. Faraday's law contour path for thin wire model.

Faraday's law model. First, the near scattered circumferential magnetic field components and the near scattered radial electric field components are assumed to vary as $1/r$ near the wire, where r is the distance from the wire center. With r constrained to be less than $0.1\ \lambda_0$ at any point in C (by FD-TD spatial resolution requirements), the $1/r$ singularity behavior of the scattered H_y and E_x fields is assumed to dominate the respective incident fields, so that the total H_y and E_x fields also take on the $1/r$ singularity. Finally, the near total H_y and the near total E_z fields, evaluated at the z midpoint of the contour, are assumed to represent the average values of their respective fields over the full z interval. These assumptions can be concisely summarized by the following expressions, assumed to apply on and within contour C of Fig. 3:

$$H_y(x, z) \simeq H_y\left(\frac{\delta}{2}, z_0\right) \cdot \frac{\left(\frac{\delta}{2}\right)}{x} \cdot [1 + c_1 \cdot (z - z_0)] \tag{6a}$$

$$E_x\left(x, z_0 \pm \frac{\delta}{2}\right) \simeq E_x\left(\frac{\delta}{2}, z_0 \pm \frac{\delta}{2}\right) \cdot \frac{\left(\frac{\delta}{2}\right)}{x} \tag{6b}$$

$$E_z(0, z) = 0 \tag{6c}$$

$$E_z(\delta, z) \simeq E_z(\delta, z_0)[1 + c_2 \cdot (z - z_0)] \tag{6d}$$

where c_1 and c_2 are arbitrary constants that need not be known.

Using the field expressions of (6a)–(6d), we can now apply the integral form of Faraday's law along contour C. We find that the $1/x$ variations in H_y and E_x yield natural logarithms. Further, the linear, odd symmetry variation in z assumed for H_y and E_z integrates out. This yields the following expression [1]:

$$\frac{H_y^{n+1/2}\left(\frac{\delta}{2}, z_0\right) - H_y^{n-1/2}\left(\frac{\delta}{2}, z_0\right)}{\delta t} \simeq \frac{\left[E_x^n\left(\frac{\delta}{2}, z_0 - \frac{\delta}{2}\right) - E_x^n\left(\frac{\delta}{2}, z_0 + \frac{\delta}{2}\right)\right] \cdot \frac{1}{2} \ln\left(\frac{\delta}{r_0}\right) + E_z^n(\delta, z_0)}{\mu_0 \frac{\delta}{2} \ln\left(\frac{\delta}{r_0}\right)} \tag{7}$$

where r_0 (assumed to be less than $0.5\ \delta$) is the wire radius. Isolation of $H_y^{n+1/2}\ (\delta/2, z_0)$ on the left side of (7) yields the required modified time-stepping relation. As stated, the analysis is easily generalized to obtain similar time-stepping relations for the other circumferential magnetic field components immediately adjacent to the wire. It should be noted that *no* other magnetic or electric field components in the FD-TD space lattice require modified time-stepping relations. All other field components are time-stepped using the ordinary free-space Yee algorithm of [13].

The accuracy of this contour integral FD-TD model is demonstrated in Figs. 4 and 5 [1]. Fig. 4 compares the FD-TD and eigenfunction expansion solutions for the circumferential magnetic field near a thin, perfectly conducting, infinitely long wire for the TM two-dimensional case. The FD-TD grid cell size is fixed at $\lambda_0/10$, while the wire radius spans a three-order of magnitude range from $\lambda_0/30\ 000$ (1/3000 cell) to $\lambda_0/30$ (1/3 cell). The field comparison point is fixed at a distance of $\lambda_0/20$ (1/2 cell) from the wire center. Excellent agreement within 2 percent is observed between the FD-TD and eigenfunction expansion solutions over the entire range of wire radius.

Fig. 5 compares the FD-TD and EFIE solutions for the circumferential magnetic field near a thin, perfectly conducting, $2.0\ \lambda_0$ long wire for the TM three-dimensional case.

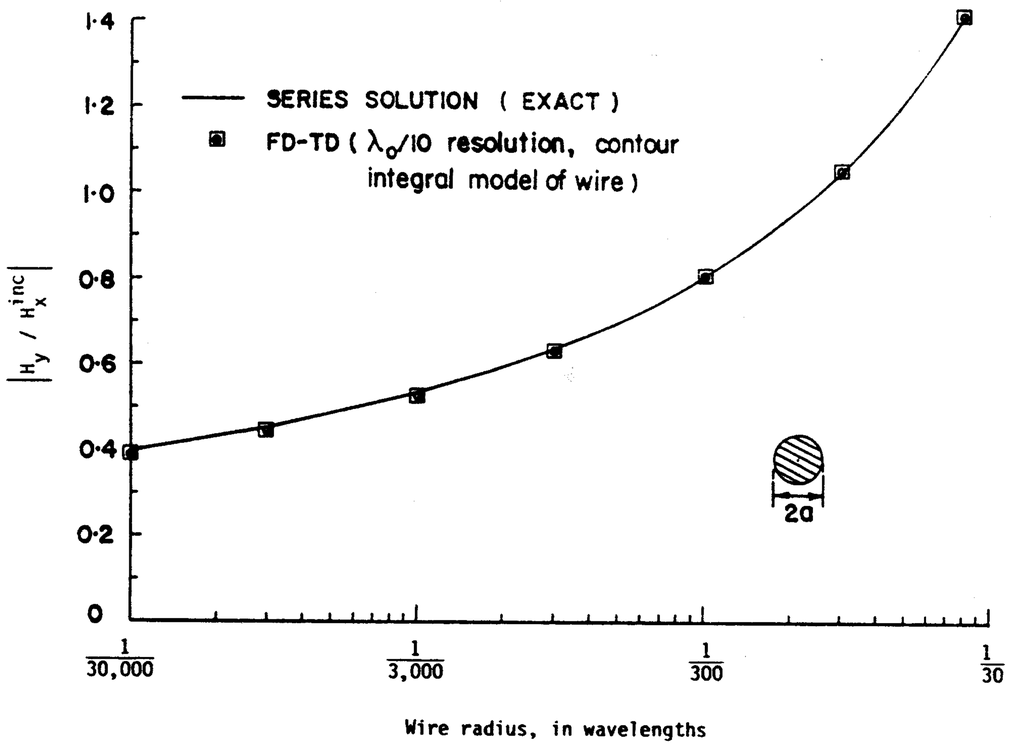

Fig. 4. Comparison of FD-TD and eigenfunction series solution for the scattered circumferential magnetic field at a point 1/20 wavelength from the center of an infinite wire.

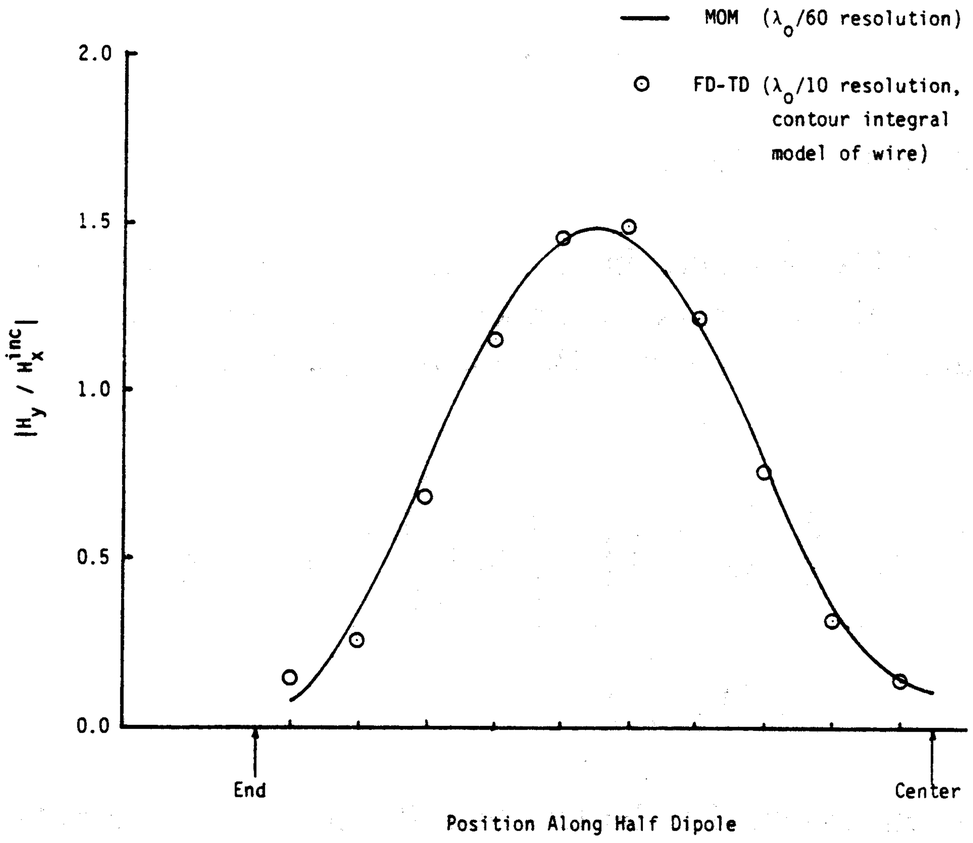

Fig. 5. Comparison of FD-TD and MM solutions for the scattered circumferential magnetic field distribution along a 2.0-Wavelength (Anti-resonant) wire of radius 1/300 wavelength (broadside TM-illumination).

Here, the FD-TD lattice cell size is again $\lambda_0/10$, but the wire radius is fixed at $\lambda_0/300$ (1/30 cell). The EFIE sampling resolution along the wire is $\lambda_0/60$; and the FD-TD/EFIE field comparison is made along the half-length of the wire (from one end to the center) at a fixed radial distance of $\lambda_0/20$ (1/2 cell) from the wire center. Excellent agreement is again noted, despite the wire current antiresonance.

IV. Virtual Surface

As stated earlier, knowledge of the total tangential E- and H-fields at all points on a closed virtual surface is sufficient to permit calculation of the total fields inside of the virtual surface. Referring to Fig. 6, the original wire bundle (and therefore the single-wire equivalence to the bundle) is assumed to be completely enclosed by a virtual surface comprised of a stack of FD-TD space cells. Each cell face, or surface patch, contains two FD-TD calculated tangential components of equivalent surface electric current and two tangential components of equivalent surface magnetic current

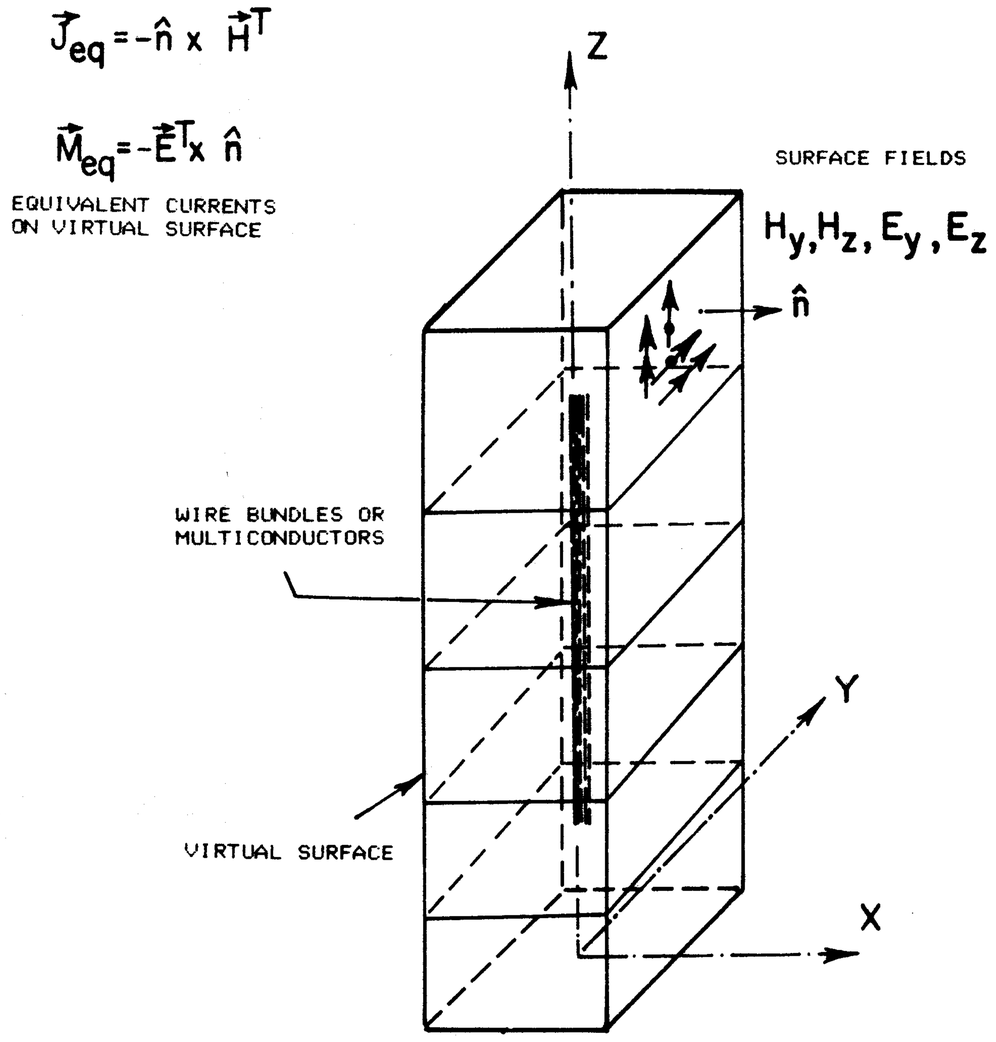

Fig. 6. Wire/wire-bundle within a closed virtual surface.

(valid for computation of internal fields) given by

$$\bar{J}_{eq}(\vec{r}) = -\hat{n} \times \bar{H}(\vec{r}) \tag{8a}$$

$$\bar{M}_{eq}(\vec{r}) = -\bar{E}(\vec{r}) \times \hat{n} \tag{8b}$$

where $\vec{r}$ is a point on the virtual surface, and $\hat{n}$ is the outward unit normal to the virtual surface at $\vec{r}$. The equivalent current sources of (8) act as the proper excitation to calculate the induced electric currents on the wires of the original bundle located within the virtual surface.

V. Electric Field Integral Equation

A complete description of the analysis of induced currents on coupled wires, with or without wire junctions, is reported in [11] based on the EFIE and the method of moments numerical technique. In shorthand notation, the EFIE is given by

$$E_l(\vec{r}) + E_l^{dr}(\vec{r}) = I(\vec{r})R(\vec{r}) \tag{9}$$

where

- $\vec{r}$ field observation point on the ith wire of the bundle
- $E_l(\vec{r})$ axially directed field at $\vec{r}$ produced by all currents on the N coupled wires of the bundle (including the self-field of the ith wire)
- $E_l^{dr}(\vec{r})$ axially directed driving field at $\vec{r}$ produced by the equivalent electric and magnetic currents on the virtual surface, given by (8)
- $I(\vec{r})$ current at $\vec{r}$, to be determined
- $R(\vec{r})$ resistance loading per unit length at $\vec{r}$.

The vector and scalar potentials used to obtain $E_l(\vec{r})$ of (9) are computed by integration of the unknown current distributions on the wires of the bundle using the thin-wire kernel function. $E_l^{dr}(\vec{r})$ is obtained by summing the surface dipole field

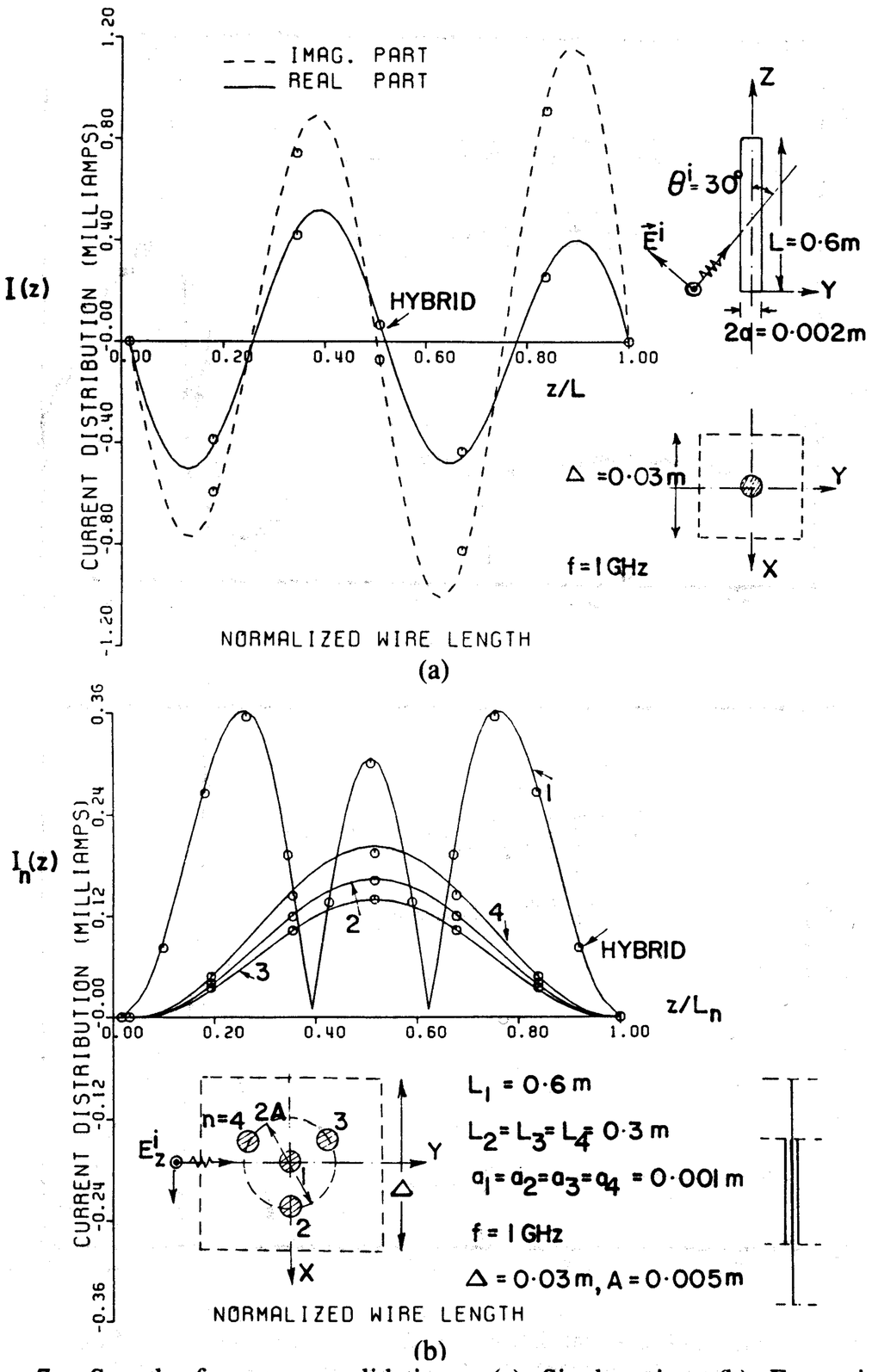

Fig. 7. Sample free-space validations. (a) Single wire. (b) Four-wire bundle, unequal wire lengths.

contributions of each square patch (FD-TD cell face) of the virtual surface, representing each patch by two constant orthogonal surface electric dipoles and two constant orthogonal surface magnetic dipoles. This involves a total of four surface integrations over each patch.

VI. Validation Studies for Wires in Free Space

Initial validation studies of the new FD-TD wire/bundle model were carried out for the case of plane wave illumination of finite-length bundles (having one to five wires) in free space. Induced currents on the wires computed using the new FD-TD model were compared to the conventional, frequency-domain EFIE solution [11]. Numerous additional validations have been made wherein the wire lengths in the bundle were made unequal. In all of these cases, the new FD-TD model provided results for the induced current distributions along the wires that are within 2 percent of the currents predicted by the pure EFIE approach, including observation points at current nulls and peaks. Selected results for the time-harmonic excitation case are reported in the following discussion.

A. Single Wire in Free Space

Referring to Fig. 7(a), this case involves a wire of length $L = 0.6$ m and radius $a = 0.001$ m, having a lumped loading of 50 Ω at its center, and illuminated by a 1 GHz plane wave at an oblique incident angle of 30° relative to the wire axis. For the FD-TD model, the wire is embedded in a 16 × 16 × 36 cell space lattice having uniform 0.03 m ($\lambda_0/10$) cubic cells.[2] A virtual surface having a single-cell cross section, and length 22 cells, surrounds the wire. For the comparative pure EFIE model, a 60 × 60 matrix solution is employed, with linear testing and pulse current expansion. As seen from Fig. 7(a), the correspondence between the FD-TD and direct EFIE solutions is within 2 percent at each observation point along the wire.

B. Multiple Wires in Free Space

Referring to Fig. 7(b), this case involves a four-wire bundle, where the center wire is of length $L_1 = 0.6$ m, and the three outer wires of lengths $L_2 = L_3 = L_4 = 0.3$ m are equispaced around a circle of radius $A = 0.005$ m. The individual wire radii, a_1, a_2, a_3, and a_4 are equal and set to 0.001 m. Plane wave illumination at 1 GHz is again assumed, but at an incident angle of 90° (broadside). For the FD-TD model, the parameters of the space lattice and virtual surface are the same as for the single-wire case, with the only change being the radius of the equivalent wire embedded within the virtual surface. Here, the equivalent wire has a varying radius corresponding to the three sections along the bundle axis. The two outer sections are 0.15 m long and have an equivalent radius of 0.001 m; while the middle section is 0.3 m long and has an equivalent radius of 0.003347 m, as calculated based on (5). As seen from Fig. 7(b), the correspondence between the FD-TD and direct EFIE solutions is again excellent (within 2 percent at all points). We note that the horizontal axis in this figure represents normalized positions along the wires of the bundle given by z/L_1 for the first wire, and z/L_n for the other three wires.

VII. Validation Studies for Wires in a Finite Cylindrical Cavity

We next consider the experimental validation of the new FD-TD wire/bundle model for the case of one and two wires within a metal cavity. Specifically, the experimental setup employed is the PLUTO (Preliminary Livermore Universal Test Object), shown in Fig. 8 [14], [15]. PLUTO is a 1.0 m high, 0.20 m diameter, cylindrical metal can above a ground plane. Approximate plane wave excitation is provided by an electrically large conical monopole referenced to the same ground plane. The aperture, usually a circumferential slot at the ground plane, has an adjustable size. Other adjustments include the position of the internal shorting plug and the position and number of the internal wires. For the cases studied, the circumferential slot aperture has 0.125 m arc length and 0.0125 m gap. The internal shorting plug is 0.40 m above the ground plane. For the one-wire study, a wire of length 0.30 m and radius 0.0004953 m is centered within PLUTO and connected to the ground plane with a lumped 50 Ω

[2] 25 s Cray-2 running time.

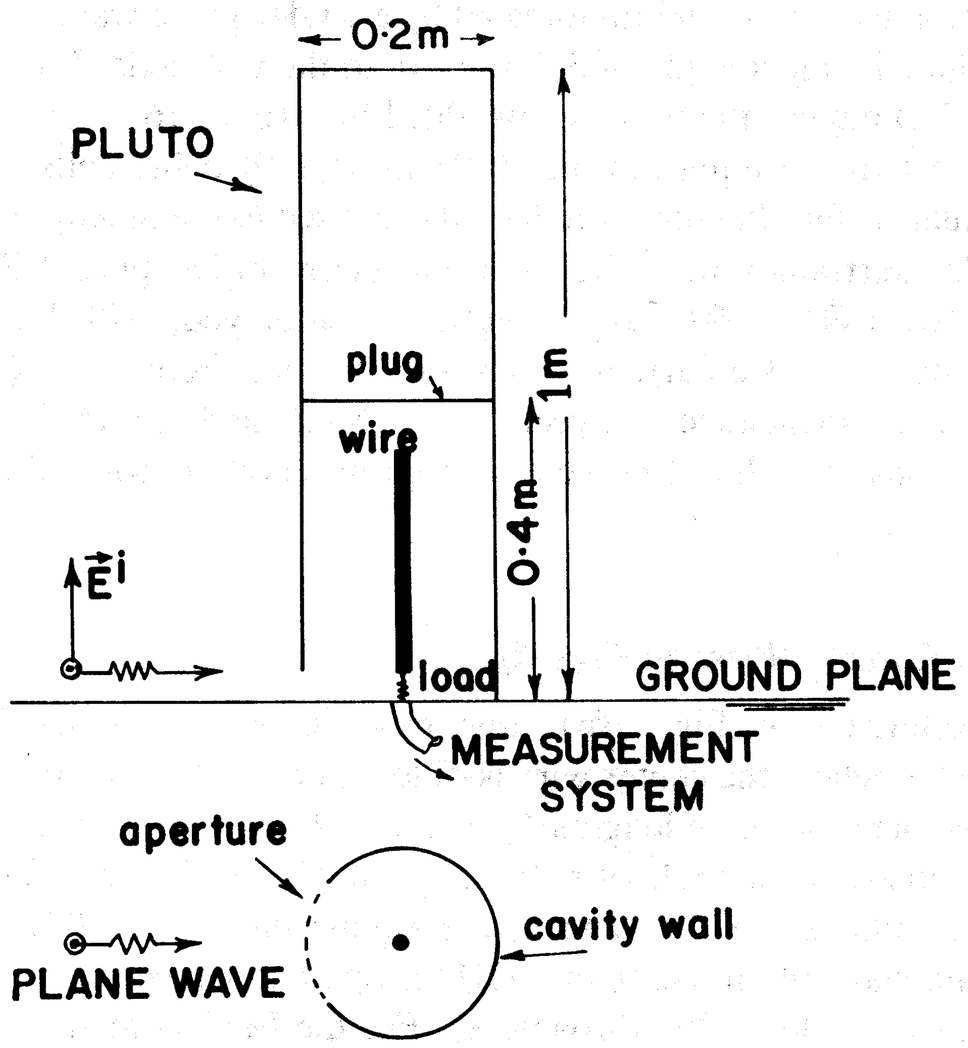

Fig. 8. PLUTO experimental geometry.

load. For the two-wire study, parallel wires of these dimensions are located 0.01 m apart at the center of PLUTO. Here, one of the wires is shorted to the ground plane, and one is connected to the ground plane with a lumped 50 Ω load. Measured data includes the magnitude and phase of the transfer function between the incident electric field and the voltage across the wire load over a wide range of UHF and microwave frequencies. The frequency range discussed here is 1.0 to 1.25 GHz, which includes a prominent coupling peak apparently due to a resonance of the slot aperture.

For the FD-TD model, PLUTO is embedded within a 16 × 32 × 88 cell space lattice. Even symmetry in both the z and x directions is exploited to minimize computer resources. Extensive convergence studies indicate that the stepped-surface FD-TD approximation of the smooth PLUTO cylinder wall and circumferential slot aperture provides a loading effect which slightly shifts the computed resonant coupling peak downward in frequency from the measured value. It is found that the bulk of this downward shift is caused by the stepped-surface approximation of the aperture, and that this frequency shift component can be eliminated by employing a Faraday's Law contour integral model to reduce the total stepped-edge length of the aperture to the desired value of 0.125 m [12]. With a lattice cell size of 0.0125 m ($\lambda_0/24$ at 1.0 GHz), the residual downward shift in the coupling peak is about 32 MHz (2.8 percent) for the single-wire case, and about 18 MHz (1.6 percent) for the two-wire case. To permit a straightforward comparison of the modeled and measured coupling response with this residual frequency shift eliminated, the lattice cell size is reduced by 2.8 percent (to 0.012144 m) and 1.6 percent (to 0.0123 m) for the two cases.

Figs. 9(a) and 9(b) compare as a function of frequency the measured and numerically modeled wire load current for the one-wire and two-wire cases, respectively, assuming a 1 V/m incident electric field. With the small residual resonance

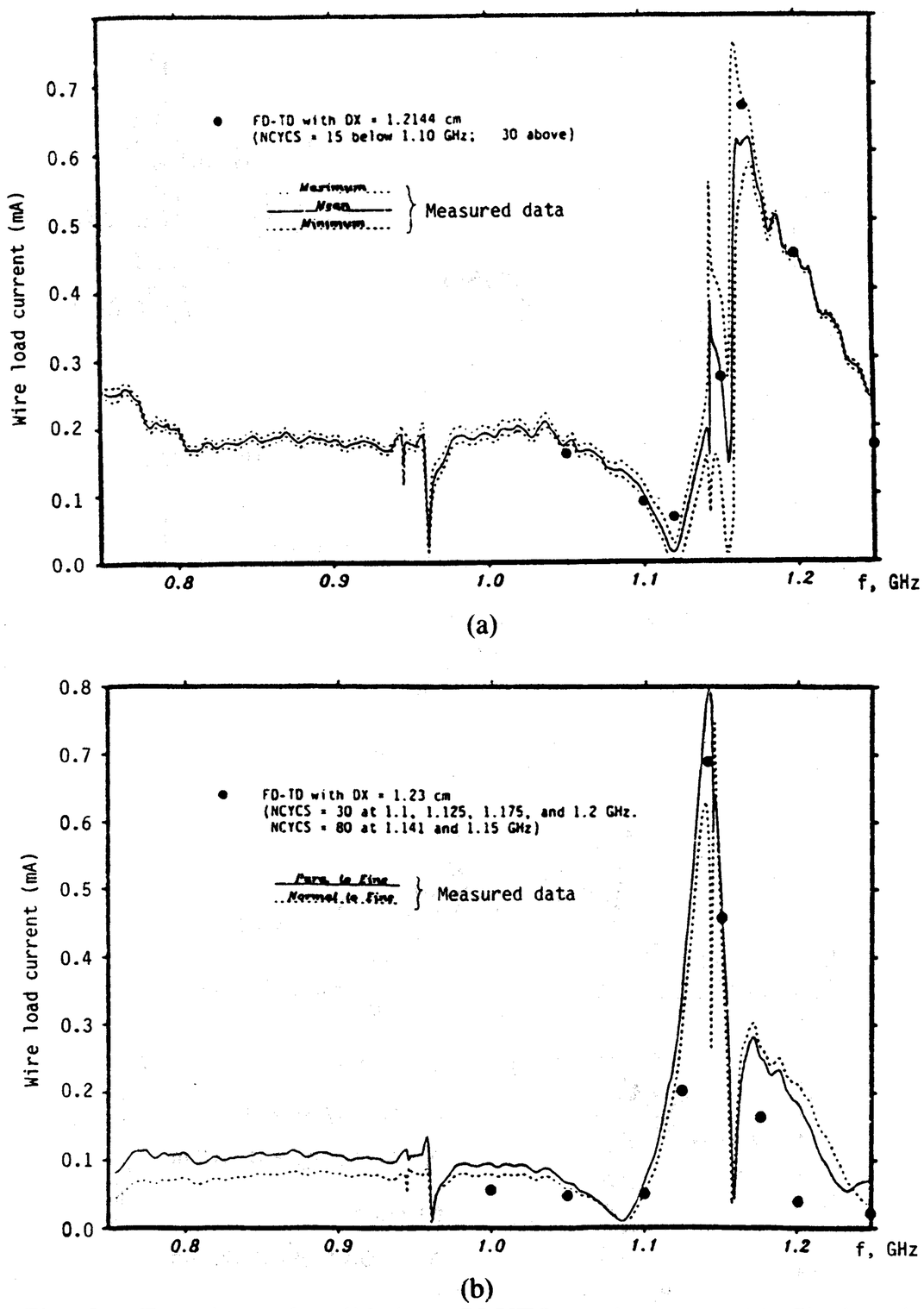

(a)

(b)

Fig. 9. Experimental validation, PLUTO cavity case. (a) Single wire centered in PLUTO. (b) Wire-pair centered in PLUTO.

frequency shift eliminated, excellent agreement is observed for both cases. Note that the two-wire case is an especially challenging test of the new FD-TD wire/bundle model, since the observed Q factor of the coupling response, defined as the center frequency divided by the half-power bandwidth, is high (approximately 75). It is found that the number of complete cycles of the incident wave required to be time-stepped to achieve the sinusoidal steady state is approximately equal to the Q factor of the resonant coupling response, for excitation frequencies near resonance. Most FD-TD runs of Fig. 9 required 30 or fewer cycles, representing a running time of about 5 min on the Cray-2 per frequency point.

Figs. 10(a) and 10(b) show the predicted detailed distribution of the induced currents on the single wire and on each of the wires of the two-wire bundle in PLUTO at their respective resonant peaks (1.166 GHz and 1.141 GHz). Only the current at the base of each wire is experimentally verified, as in Figs. 9(a) and 9(b). Figs. 10(a) and 10(b) are included since little data has been published concerning coupling to wires in three-dimensional cavities.

VIII. Validation Study for Broad-Band Excitation

A validation study was conducted for the new FD-TD wire/bundle model applied to model the transient (nontime-

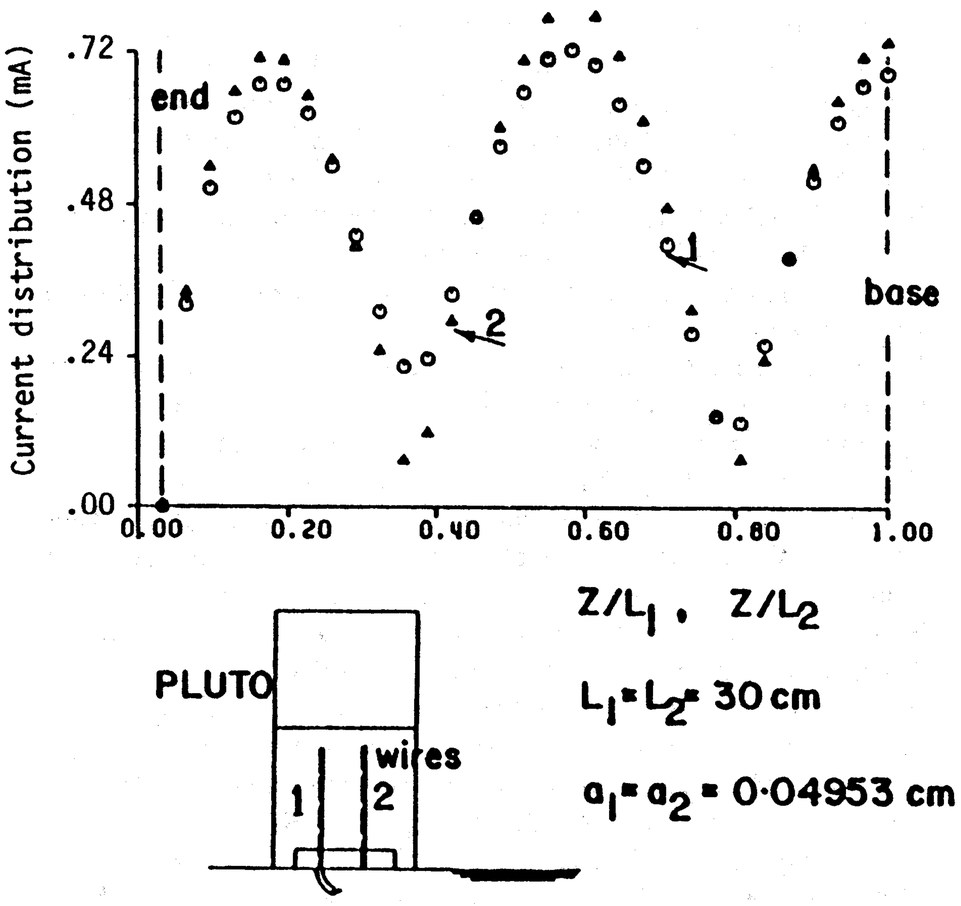

(a)

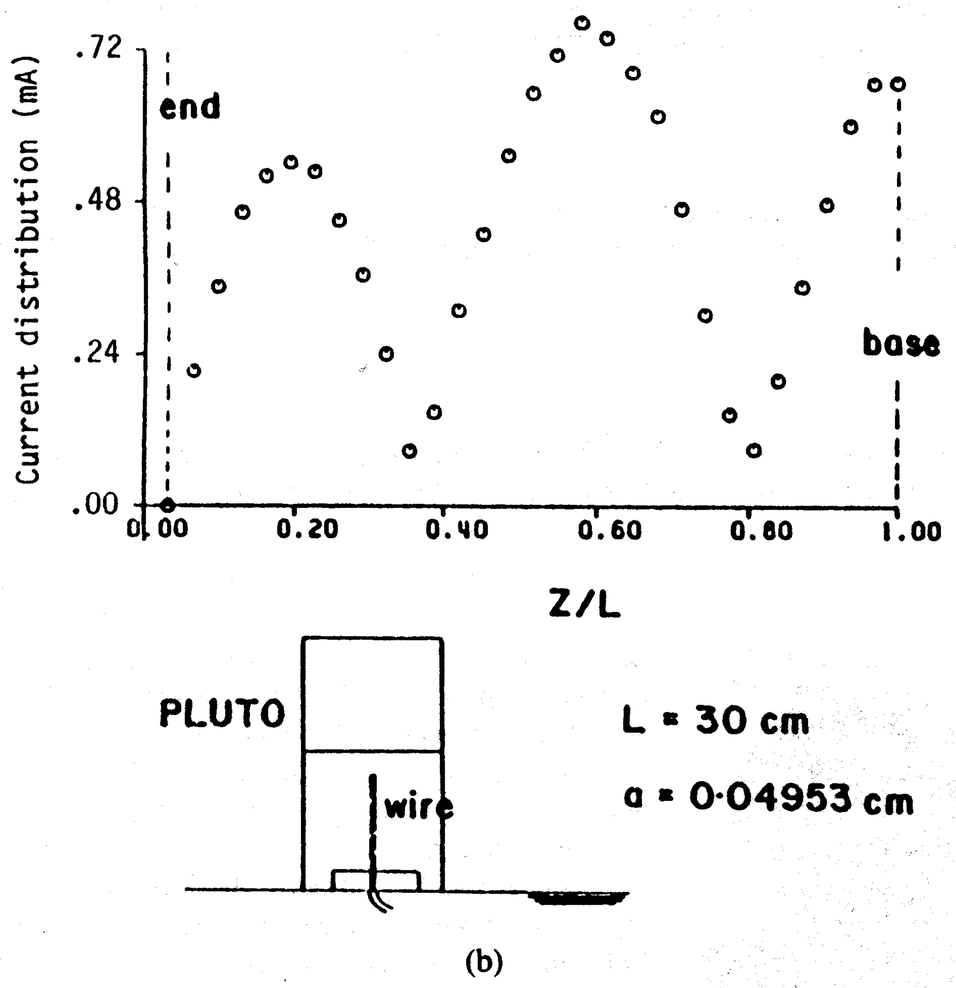

(b)

Fig. 10. FD-TD predicted induced current distributions, PLUTO cavity case. (a) Along single wire centered in PLUTO. (b) Along each wire of the wire-pair centered in PLUTO.

harmonic) excitation of a single wire in free space. Here, the goal was to determine whether a single FD-TD run, using a properly chosen plane wave pulse, could provide sufficiently accurate field versus time data at a virtual surface surrounding a wire so that the induced wire current could be determined over a wide spectrum of frequencies using the Fourier transform of the virtual-surface fields. This would cut the overall computer time needed to characterize broad-band coupling by perhaps more than one order of magnitude.

The wire modeled is of length $L = 0.6$ m and radius $a = 0.0004955$ m, having a lumped loading of 50 Ω at its center, and illuminated by a TM-polarized plane wave at broadside incidence. The illuminating wave is assumed to be a 1 GHz carrier double-sideband (DSB) modulated by a Gaussian pulse

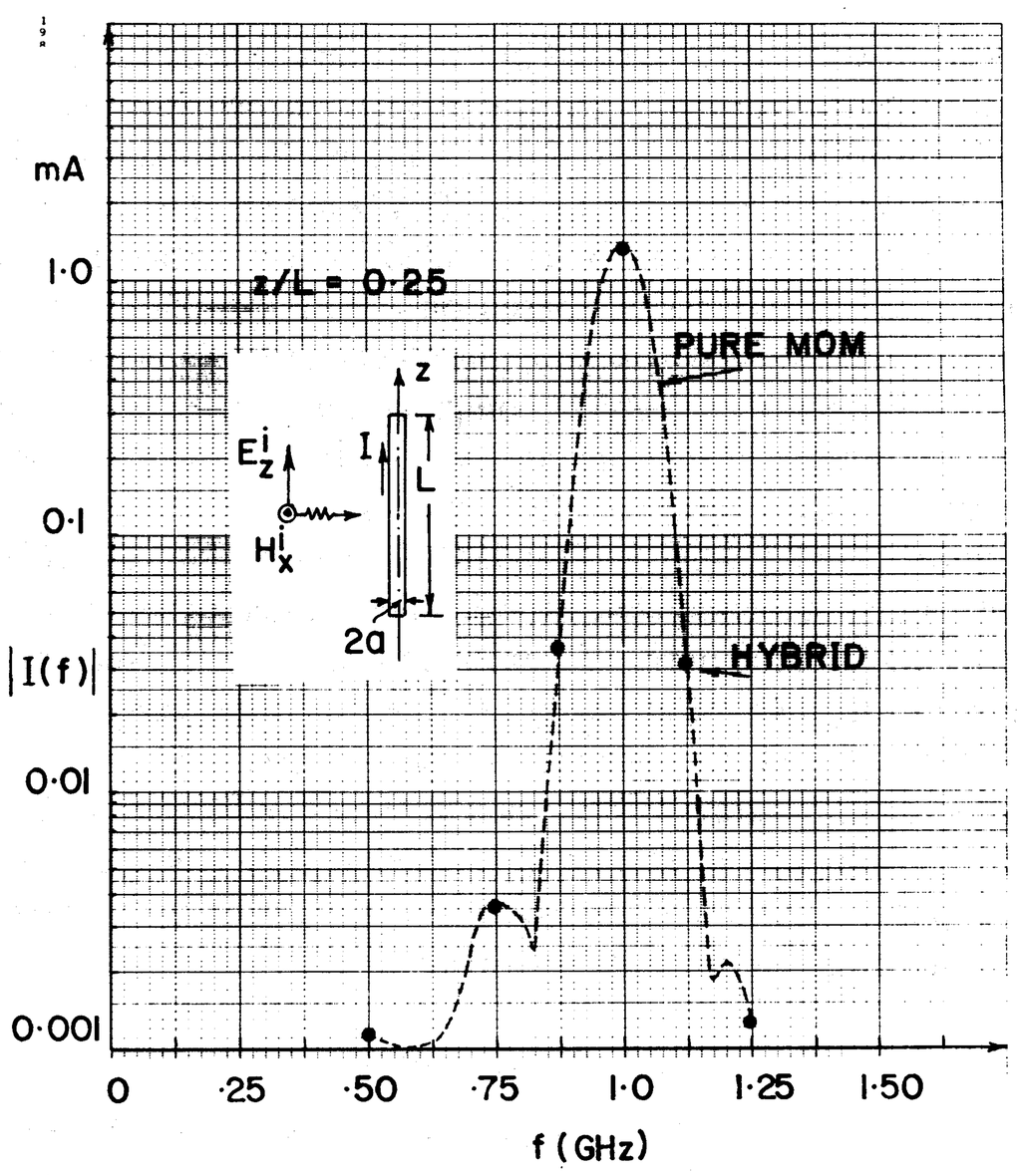

Fig. 11. Validation of predictions of single broad-band FD-TD run for induced wire current versus frequency.

having a 5 ns characteristic decay time. For the FD-TD model, the parameters of the space lattice and virtual surface are the same as for the single-wire case of Section VI. The FD-TD code is modified only in the use of the modulated pulse excitation, storage of time histories of the tangential E and H components at each square patch of the virtual surface, and addition of a Fourier transform routine to obtain the complete spectrum of the total fields on the virtual surface from the stored time histories. At each frequency of interest, the magnitude and phase of these fields are used as inputs to the EFIE subroutine, which then proceeds in a manner identical to that employed previously for the single-frequency, time-harmonic excitation FD-TD case.

Fig. 11 graphs as a function of frequency the induced electric current on the wire at an observation point one-fourth of its total length from one end. The results of the single, broad-band-excitation FD-TD run are seen to be in excellent agreement with data obtained from multiple runs of a conventional, frequency-domain, EFIE code using the method of moments. It is seen that useful coupling data is obtained over a frequency band substantially broader than the nominal 0.9-1.1 GHz bandwidth of the modulated pulse used as the FD-TD excitation, and over three orders of magnitude of current values. With 40 frequency points provided by the single, broad-band FD-TD run, it is found that the Cray-2 running time per frequency point is reduced by a factor of 90 percent from the time-harmonic excitation FD-TD case of Section VI (to only about 2.5 seconds per frequency point).

IX. Summary and Conclusion

This paper has presented an efficient numerical technique for the calculation of induced electric currents on coupled

wires or wire bundles placed in an arbitrary shaped cavity and excited by an external plane wave. The concept of equivalent radius has been used to replace a possibly complex wire bundle with a single wire in the FD-TD model. The radius of the equivalent wire can be accounted by a modified FD-TD time-stepping expression (based on a Faraday's law contour path formulation) for the looping magnetic fields adjacent to the equivalent wire. FD-TD computed total fields at a virtual surface fully enclosing the equivalent wire are then obtained, permitting calculation of the currents on the wires of the original bundle using a standard frequency-domain EFIE. Substantial numerical and experimental validations have been reported for time-harmonic excitation of wires in free space and in a high-Q metal cavity. A representative study is also presented for a broad-band excitation of a wire in free space in order to demonstrate an approach to obtain multiple-frequency results with one FD-TD run. It is concluded that the method of this paper provides a powerful tool for modeling important physics of electromagnetic wave coupling.

Acknowledgment

The authors wish to thank Dr. W. Travis White, Dr. Kane S. Yee, and Dr. Hriar Cabayan of Lawrence Livermore National Laboratory for their technical assistance, encouragement, and support.

References

[1] A. Taflove, K. R. Umashankar, B. Beker, and F. Harfoush, "Detailed FD-TD analysis of electromagnetic fields penetrating narrow slots and lapped joints in thick conducting screens," *IEEE Trans. Antennas Propagat.,* to be published.

[2] C. M. Butler and K. R. Umashankar, "Electromagnetic excitation of a wire through an aperture-perforated conducting screen," *IEEE Trans. Antennas Propagat.,* vol. AP-24, pp. 456–462, July 1976.

[3] K. R. Umashankar and J. R. Wait, "Electromagnetic coupling to an infinite cable placed behind a slot-perforated screen," *IEEE Trans. Electromagn. Compat.,* vol. EMC-20, pp. 406–411, Aug. 1978.

[4] Y. Naiheng and R. F. Harrington, "Electromagnetic coupling to an infinite wire through a slot in a conducting plane," *IEEE Trans. Antennas Propagat.,* vol. AP-31, pp. 310–316, Mar. 1983.

[5] R. W. Ziolkowski and R. F. Schmucker, "Scattering from a slit cylinder enclosing an off-set impedance cylinder," in *Proc. 1986 Nat. Radio Sci. Meet. (URSI),* Philadelphia, PA, June 1986, p. 122.

[6] A. Taflove and K. R. Umashankar, "A hybrid moment method/finite-difference time-domain approach to electromagnetic coupling and aperture penetration into complex geometries," *IEEE Trans. Antennas Propagat.,* vol. AP-30, pp. 617–627, July 1982.

[7] R. Holland and L. Simpson, "Finite-difference analysis of EMP coupling to thin struts and wires," *IEEE Trans. Electromagn. Compat.,* vol. EMC-23, pp. 88–97, May 1981.

[8] S. A. Schelkunoff, "Field equivalence theorems," *Comm. Pure Appl. Math.,* vol. 4, pp. 43–59, June 1951.

[9] R. W. P. King, *The Theory of Linear Antennas.* Cambridge, MA: Harvard Univ. Press, 1956.

[10] K. R. Umashankar and C. E. Baum, "Equivalent electromagnetic properties of a concentric wire cage as compared to a circular cylinder," *Sensor and Simulation Notes,* Note 252, Air Force Weapons Laboratory, Kirtland AFB, NM, Mar. 1979.

[11] C. M. Butler, K. R. Umashankar, and C. E. Smith, "Theoretical analysis of the wire biconical antenna," U.S. Army Stratcom, Fort Huachuca, AZ, Tech. Rep. PCN-18-74, Jan. 1975.

[12] T. G. Jurgens, A. Taflove, and K. R. Umashankar, "Conformal FD-TD modeling of objects with smooth curved surfaces," in *Proc. 1987 Nat. Radio Sci. Meet. (URSI),* Blacksburg, VA, June 1987.

[13] K. S. Yee, "Numerical solution of initial boundary value problems involving Maxwell's equations in isotropic media," *IEEE Trans. Antennas Propagat.,* vol. AP-14, pp. 302–307, May 1966.

[14] R. J. King, J. K. Breakall, H. G. Hudson, J. J. Morrison, V. G. McGevna, K. S. Kunz, A. P. Ludwigsen, and D. K. Gnade, "Phenomenology of microwave coupling, Part I," Lawrence Livermore Nat. Lab., Livermore, CA, Rep. UCID-20215, Nov. 1984.

[15] R. J. King, A. P. Ludwigsen, and K. S. Kunz, "Phenomenology of microwave coupling, Part II," Lawrence Livermore Nat. Lab., Livermore, CA, Rep. UCID-20215, Part 2, Aug. 1985.

Korada R. Umashankar (S'69–M'75–SM'81), for a photograph and biography please see page 765 of the June 1986 issue of this TRANSACTIONS.

Allen Taflove (M'75–SM'84), for a photograph and biography please see page 766 of the June 1986 issue of this TRANSACTIONS.

Benjamin Beker (S'86) was born in Vilnius, Lithuania, in 1959. He received the B.S.E.E. and M.S.E.E. degrees in 1982 and 1984, respectively, from the University of Illinois at Chicago (UIC), where he is currently pursuing a Ph.D.

Since 1982 he has been working as a research assistant in the Department of Electrical Engineering and Computer Science. His interests include EM field interaction with material bodies, computational methods, and applied mathematics.